Capabilities and limitations of advanced optical satellite missions for snow, vegetation, and artificial light source applications in Arctic areas

Alison Beamish, Christopher C.M Kyba, Jacqueline Coesfeld, Sabine Chabrillat (GFZ German Research Centre for Geosciences); Roberto Salzano (CNR National Research Center of Italy, Institute of Atmospheric Pollution Research); Rosamaria Salvatori (CNR National Research Center of Italy, Institute of Polar Sciences)

Potsdam, Germany, 25 November 2019

WP3: Satellite remote sensing of Arctic surfaces

Task 3.2: Optical satellite remote sensing

Deliverable 3.2.1: A technical report on the assessment of the capabilities and limitations of advanced optical satellite missions for snow, vegetation, and gas flaring mapping applications in Arctic areas

1 Introduction

A greater understanding of the phenomenon of Arctic climate change and amplification has led to intensive and conclusive research of Arctic ecosystem change over the last 50 years (see IPCC, 2014; AMAP 2017). Climate warming has resulted in cascading changes to terrestrial ecosystems including snow cover extent and depth, shifting vegetation composition, productivity, and phenology, as well as increased sensitivity to natural and anthropogenic disturbance (Bhatt et al., 2010; Chapin et al., 2005; Elmendorf et al., 2012; Serreze et al., 2000).

Optical remote sensing is an invaluable tool to monitor terrestrial Arctic change at multiple spatial scales. Recent advances in sensor technology of legacy and new platforms has resulted in greater availability of high spectral resolution optical satellite data such as the broadband Landsat 8 OLI and Sentinel-2 mission, as well as the current and upcoming hyperspectral missions of PRISMA and EnMAP, respectively.

In the following report, we demonstrate how advanced optical remote sensing technologies supported by in-situ validation data can be used to monitor and map (1) snow properties and snow melt regimes; (2) vegetation biomass, activity and biodiversity; and (3) the source and intensity of artificial light in the Arctic through night light observations.

2 Snow mapping

2.1 Background

Snow cover is an important component of the cryosphere that plays a key role for climate dynamics and the resources availability: the seasonality of the snow cover influences weather patterns, hydro-power generation, agriculture, forestry, tourism, and aquatic ecosystems (Beniston et al., 2018). The snow cover characterization and its annual spatial-evolution represent important factors to be considered in the framework of climate modelling at a global scale. Furthermore, the snow cover has been officially declared as an Essential Climate Variable (ECV) by the Global Climate Observing System (GCOS) and high priority is assigned to enhancing and maintaining snow cover observations (WMO, 2010; 2011). From this perspective, the continuous monitoring of snow covers is a major challenge of these last years and the advances in remote sensing explain why optical data are so diffusely used to monitor the snow covers. The description of the snow cover implies two variables: the extent and the albedo. Remote sensing is the most common tool for the routine estimation of the snow cover extent. However, two different aspects must be considered for the enhancement of the final output: time and spatial resolutions. Both components, using remotely sensed data, are connected to each other, since the higher the spatial resolution (below hundreds of meters), the lower the revisit time interval (more than 1 week) (Dietz et al., 2012). Concerning the albedo, the spectral behaviour of the snow reflectance in the visible and short-wave infrared ranges supports the discrimination of snowed surfaces from other matrices and, moreover, the characterization of the snow surface (Painter et al., 2003; Tedesco & Kokhanovsky, 2007). In details, the reflectance of pure snow in the visible range of the electromagnetic spectrum (400–700 nm) is approximately 100 % and it decreases as a function of the amount of impurity content in the snow and slightly increasing in the size of the snow grains with ageing (Figure 2-1). In the short-wave infrared part of the solar spectrum (700–2500 nm), snow reflectance decreases rapidly and it is mostly controlled, in this case, by the snow grain size (Warren & Wiscombe, 1980; Wiscombe & Warren, 1980; Warren, 1982). The major advantage to monitor the snow with remote sensed data is the possibility to derive area-wide and spatially comprehensive surface information with a regular repeatability of measurements, even in remote areas. However, some limitations can occur when cloud cover or vegetation are present. While clouds avoid only to analyse the underlying surface, vegetation can produce omission and/or commission errors. Additional problems could affect the results in mountain areas where the surface heterogeneity is consistent.

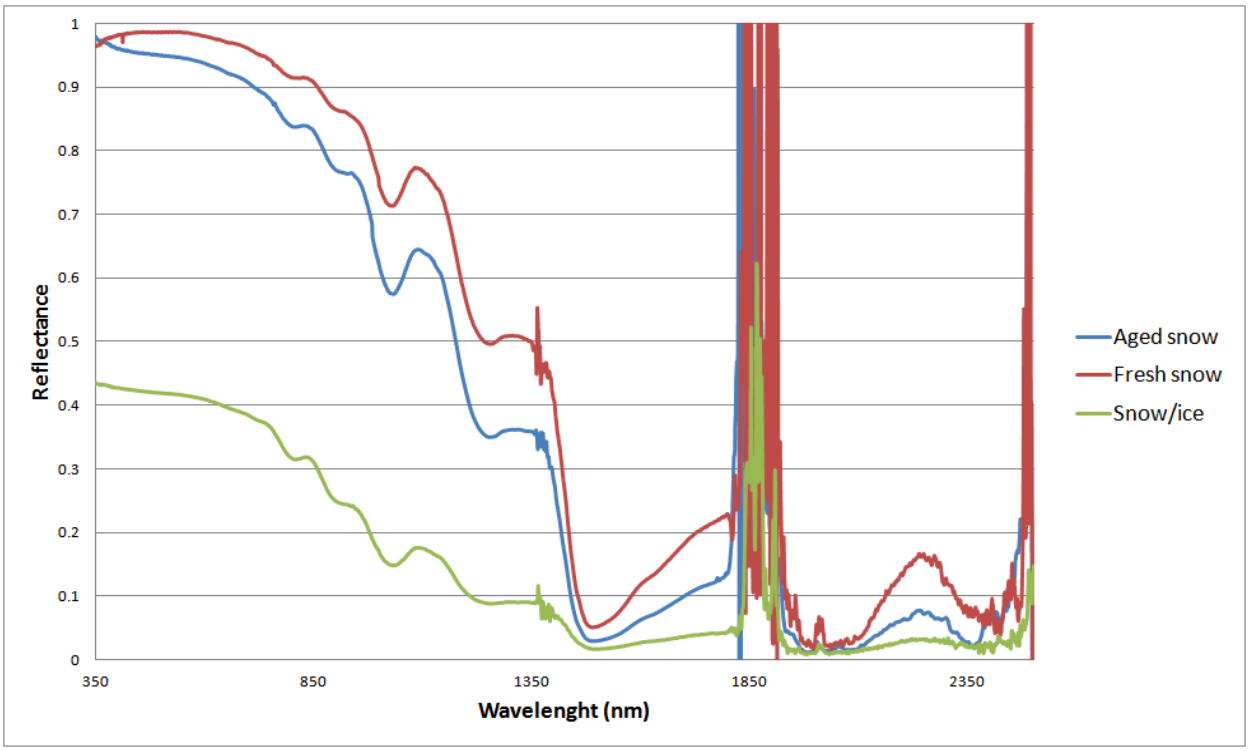

Figure 2-1 Spectral behaviour of different snow covers

The state-of-the-art snow products concerning the snow extent are derived using remotely sensed data and they are based mainly on multispectral optical sensors. They can investigate the snow cover and give information about the size and the shape of snow grains (Dozier et al., 2009), the presence of impurity soot, the age of the snow, and the presence of depth hoar. Furthermore, the short-wave infrared signal can support the discrimination between snow and clouds (Rodell et al., 2004). Considering that snow-covered surfaces are highly reflective in the visible range and low reflective in the short-wave infrared (swir) (Salomonson & Appel, 2006), it is possible to define an index that enhances the discrimination between snow and not snow in a single pixel. This index, defined as Normalized Difference Snow Index (NDSI), is calculated as follows:

$$NDSI = (R_G - R_{swir})/(R_G - R_{swir}) \quad (1)$$

The green and the swir parameters are the bands available for each satellite sensor and their selection includes generally wavelength ranges centered at 500–600 nm (R_G) and 1500–1600 nm (R_{swir}). The estimation of the snow extent from remotely sensed multispectral images is based on the relation between the radiative behavior of the surfaces and the Fractional Snow Cover (FSC). This parameter describes the percentage of surface covered by snow (Painter et

al., 2009) in a pixel element of a remotely sensed image. The relation between the FSC and the NDSI represents the most common inference required by remote sensing studies. There are two options for estimating the NDSI—FSC relation: the first one consists in combining satellite products with different spatial resolution (Yin et al 2013); and the second one can be approached having a ground truth information. The first solution is based on (Salomonson & Appel, 2006) combining Landsat and MODIS data and a NDSI to FSC relation is defined.

$$FSC = 1.45 \times NDSI - 0.01 \quad (2)$$

This knowledge is implemented in the SNOWMAP algorithm (Hall et al., 2016), which is the core of the MODIS data chain for the definition of remotely sensed snow products. This approach is replicated also on Landsat data (Vermote et al., 2016) and in the NASA VIIRS ATBD (Riggs et al., 2015), derived by Suomi NPP satellite platform. Similarly, it is included in the SC algorithm, which is part of the Sentinel 2A data chain (Main-Korn et al., 2017). The second solution can be approached defining an empirical reflectance-to-snow-cover model that requires a calibration having a number of reference sites in the satellite image. The most important example is the so-called Norwegian Linear Reflectance-to-snow-cover algorithm (NLR) (Solberg et al., 2006) that is the core of the GlobSnow Snow Extent (SE) data chain (Metsämäki et al., 2015). From this perspective, the availability of webcam networks is an important data source for calibration and validation processes. The attention of the scientific community of this proxy is increasing, and the literature about this topic is growing (Salzano et al., 2019).

Several satellite products are available for the remote sensing of the cryosphere and for this study we considered products obtained by optical sensors, characterized by different spatial resolutions: high (< 100 m); intermediate (100 m - 1 km); and low (> 1 km). The integration between those products and ground-based imagery will be tested, in order to improve the dataset concerning the snow cover over a decade.

The available remotely sensed snow products with a higher spatial resolution (< 100 m) were limited to the Landsat and the Sentinel-2 missions (Table 2-1). While Landsat data are available since 2004 with a revisiting time of about 16 days, the Copernicus program provides imagery only since 2015 with a revisiting time passed form 10 days to about 5 days since 2017 after the launch of a second platform. While the Landsat satellites are characterized by a spatial resolution up to 30 m, the Sentinel sensors are featured by a spatial resolution ranging from 10 to 60 m. The available data must be geometrically and atmospherically corrected and different tools must be considered in order to prepare a 2A level product. Possible solutions are based on

using the Second Simulation of the Satellite Signal in the Solar Spectrum (6S) algorithm available in the Atmospheric and Radiometric Correction of Satellite Imagery (ARCSI) software (Vermote et al., 1997) or the Sen2Cor toolbox (ESA, 2018). The final estimation of NDSI was possible considering Eq.1 and the first short-wave infrared band of Landsat sensors. The wavelength ranges are specific for each sensor and they correspond to 520–600 nm and 1550–1755 nm for missions 5 and 7, and 533–590 nm and 1566–1651 nm for mission 8 (Barsi et al., 2014), 543-578 nm and 1565-1655 nm for the Sentinel 2A platform.

The highest time resolution available for optical remote sensing is provided, in the framework of the Earth Observing System (EOS) flagship, by NASA's satellites Suomi NPP, Terra and Aqua. Terra and Aqua are both equipped with the Moderate Resolution Imaging Spectroradiometer (MODIS) and they provide the coverage of the Earth two times daily (Terra in the local morning and Aqua in the local afternoon). The instrument is characterized by 36 bands with a spatial resolution of 250 m in the visible range and 500 m in the short-wave infrared. The Suomi NPP platform is equipped by the Visible Infrared Imaging Radiometer Suite (VIIRS), 22-band radiometer, which is similar to MODIS (satellites Aqua and Terra), but with better facilities (the spatial resolution is up to 375 m). The NASA's data chain provides the retrieval of NDSI at the ground for Suomi NPP, Terra and Aqua (Hall et al., 2016). The NDSI values can be calculated using in the Equation 1 the MODIS bands 4 (545–565 nm) and 6 (1628–1652 nm) or the VIIRS band 1 (0.64 μm) and band I3 (1.61 μm).

Finally, the daily estimation of the snow cover extent is being provided, over the considered period, by the European Space Agency as a component of the Data User Element. The GlobSnow Snow Extent (SE) product covers the Northern Hemisphere and the processing data chain combines optical measurements in the visual and in the thermal part of the electromagnetic spectrum acquired by the ERS-2 sensor ATSR-2 and the Envisat sensor AATSR. Since 2016 the product has been extended to the Suomi NPP data.

The first step of the data chain is based on a cloud-cover retrieval algorithm (SCDA) where clouds, as well as large water bodies (oceans, lakes and rivers) and glaciers, are masked out. This algorithm is based on the brightness - temperature difference between 11 and 3.7 μm and on a set of additional rules, useful for certain sky conditions. Furthermore, the snow cover information is retrieved for not-vegetated areas by the NLR algorithm (Metsämäki et al., 2012) where the band 2 (670 nm) is considered. This step is based on a semi-empirical reflectance model, where reflectance from a target is expressed as a function of the snow fraction. The Fractional Snow Cover can then be derived from the observed reflectance based on the given

reflectance constants and the transmissivity values. The product is provided daily with a spatial resolution of 1 km and the data are available using the GlobSnow service (Metsämäki et al., 2015).

Table 2-1 Summary of the available snow products obtained by remote sensing at high latitudes

Product	Platform	Sensor	Spatial resolution (m)	Revisit time (days)	Year	Algorithm
Globsnow SE	ERS-2 Envisat Suomi NPP	ATSR-2 AATSR VIIRS	1000	7	1995 - 2002 2002 - 2012 2016 - ongoing	SCAMod NLR
MODIS SCF	Terra Aqua	MODIS	500	0.5	1999 - ongoing 2003 - ongoing	SNOWMAP
VIIRS SC	Suomi NPP	VIIRS	375	1	2012 - ongoing	SNOWMAP
Landsat SCA	Landsat 5 Landsat 7 Landsat 8	TM ETM+ OLI	30	16	1984 - 2013 1999 - ongoing 2013 - ongoing	SNOWMAP
Sentinel SC	Sentinel-2A Sentinel 2B	OLCI MSI	10	5	2015 - ongoing 2017 - ongoing	Level 2A - SC

2.2 Case study

We selected a study area located close to Ny-Ålesund (Svalbard - Norway) where the Italian Arctic Station represents an important scientific facility and experimental activities are appropriately supported. The site is characterized by intense international research collaborations and different data sources can be included as input for the integration between remotely sensed data and terrestrial images collected by webcam. We performed an overview about the algorithms focused on processing multispectral images and snow index calculation as well as on the automatic geo-rectification of ground-based photography and on the routinely estimation of the fractional snow cover. We considered satellite product characterized by intermediate (MODIS) and high (Sentinel-2) spatial resolutions and we investigated the relation

between FSC and NDSI under different snow cover conditions. The aim of this first part of activities was focused on estimating omissions and commissions between automated algorithms and supervised classifications. The selected MODIS product is part of the USGS data-chain concerning the snow cover and it provides an NDSI estimation with a spatial resolution of 500 m twice per day. On the other hand the Sentinel-2 reflectance product was obtained using the Sen2Cor processor and it is characterized by a 10 m spatial resolution available since 2017 every 5 days. While the automated algorithm was based on selecting a NDSI threshold of 0.6 as discriminating factor between snowed and not-snowed pixels, the supervised approach was supported by the definition of different region-of-interest (ROI) and by the estimation of a "distance" parameter that assess the type of land cover. We used the maximum likelihood distance as estimator and we defined different ROIs: snow, shadowed snow, cloud covered snow, and bare soil. Both approaches were carried out on Sentinel data in order to minimize the mixing pixel effect and we report here a couple of examples that summarize the most important issues (Figure 2-2).

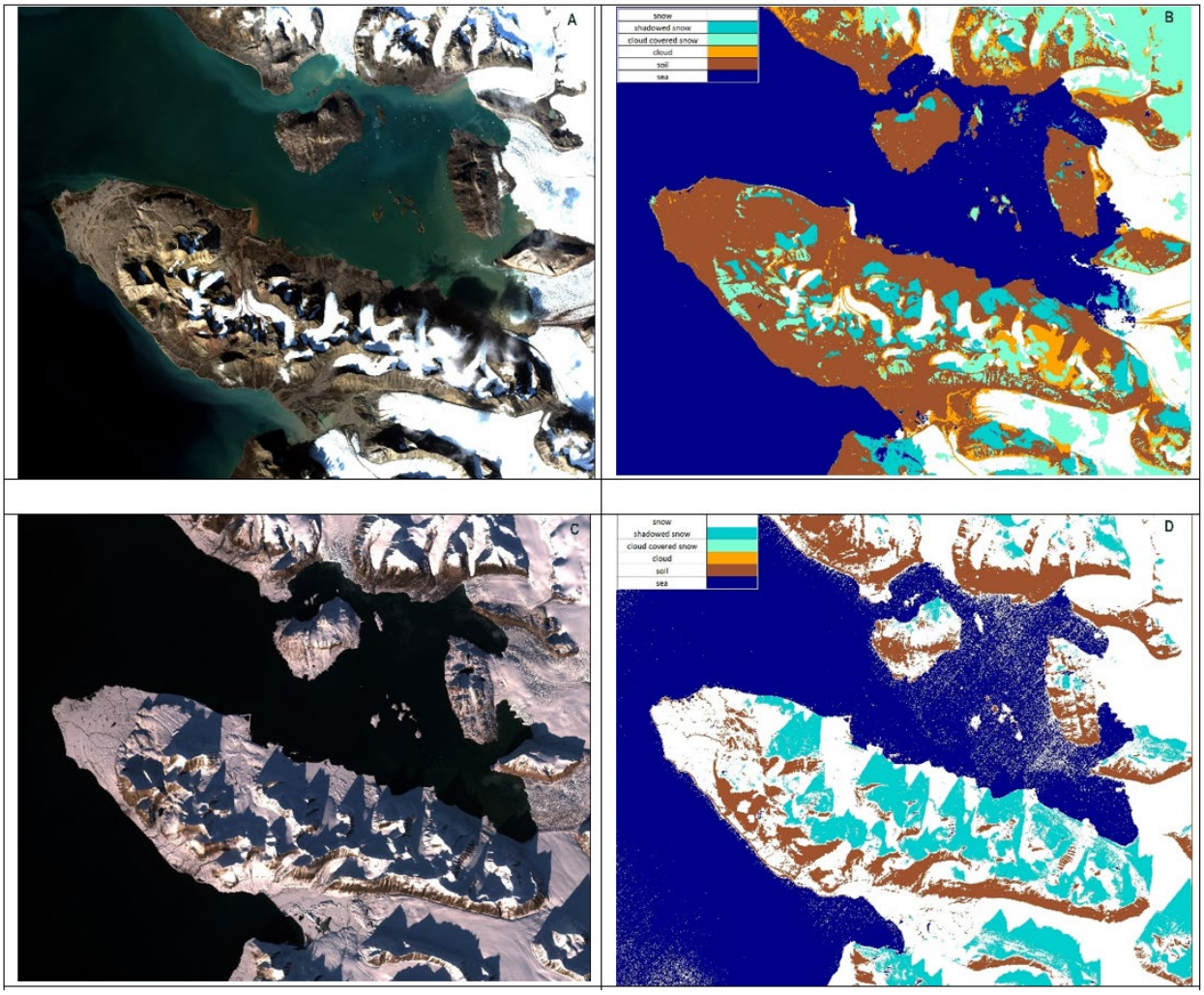

Figure 2-2 The snow cover at Ny-Ålesund during two different seasons: (A) August 20th 2018; (B) September 17th 2018. Relationship between the spectral index of snow (NDSI) obtained by Sentinel data and the classification obtained using supervised classifications (C,D).

Table 2-2 Identification of surface cover types using supervised and automated classifications

	August 20th 2018		September 17th 2018	
Class	**NDSI > 0.6 [%]**	**Total [%]**	**NDSI > 0.6 [%]**	**Total [%]**
Snow	99.8	22.4	100	8.6
Shadowed snow	32.3	8.2	98.9	68.2
Cloud-covered snow	67.7	16.0	30.4	19.8
Soil	0.7	53.5	79.4	3.4

Looking at the comparison between the two different approaches we can highlight a good agreement under clear and illuminated conditions of the surface but we can detect a significant underestimation in shadowed and partially-cloud covered areas (Table 2-2). These areas represent in August about 25% of the total area corresponding to the Kongsfjorden bay. Such an effect appeared to be limited in September when snow cover started to be almost complete and misclassification are lower than 10%. Considering that intense cloud cover is recurrent (up to 80% of cloudy conditions per year) in Svalbard islands (Salzano et al., 2016), the availability of Sentinel data is limited and the use of intermediate spatially-resolved imagery is required. MODIS data are unfortunately affected by the mixing pixel and the availability of ground-truth is an important issue. The state-of-the-art approaches are based on integrating MODIS imagery with Landsat or Sentinel data. We considered in our case study the same Sentinel images of the previous exercises and we compared in this experiment the Sentinel-derived FSC to the MODIS NDSI product (Figure 2-3).

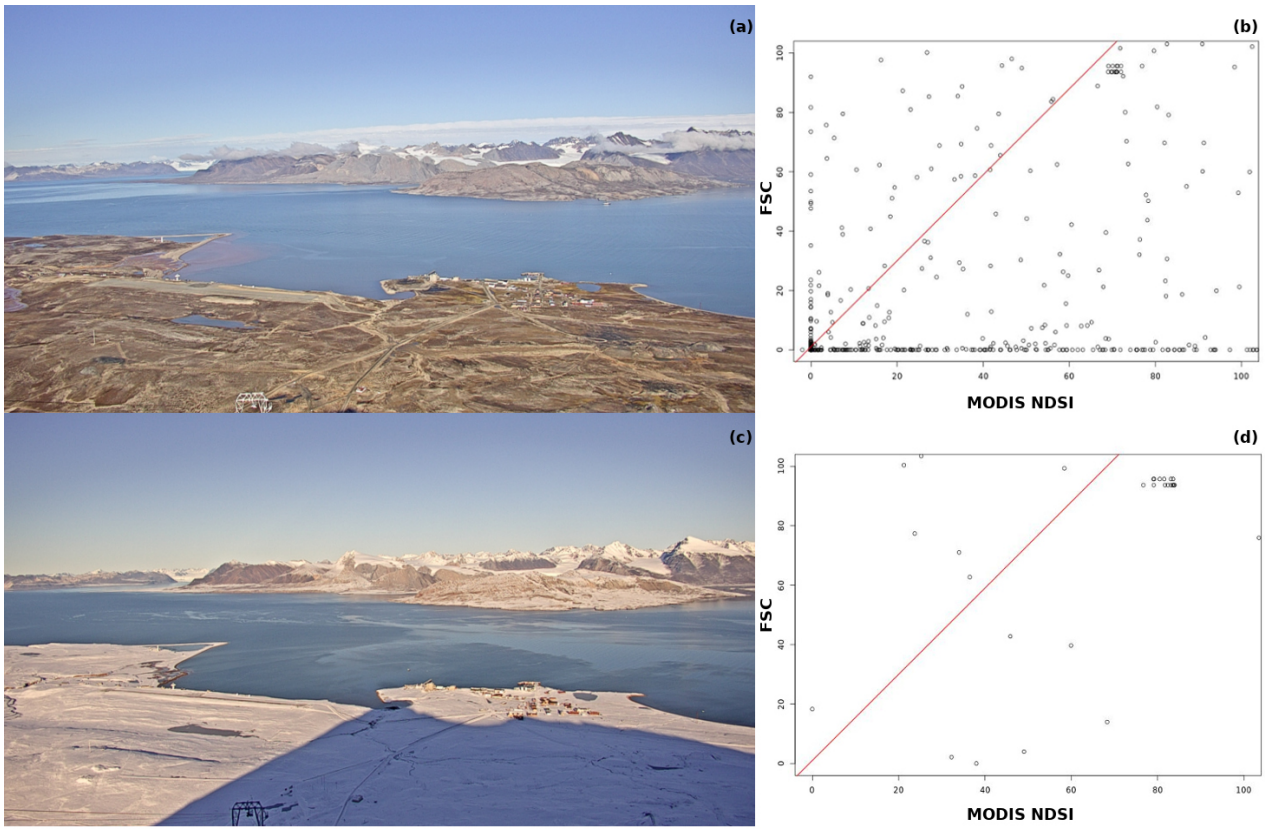

Figure 2-3 The snow cover at Ny-Ålesund during two different seasons: (a) August 20th 2018; (c) September 17th 2018. Relationship between the spectral index of snow (NDSI) obtained by MODIS data, and the Fractional Snow Cover estimated by Sentinel data ((b),(d)).

The obtained FSC-to-NDSI relations were coherent to the Salomonson & Appel (2006) in September and some problems were detected in August. These observations are influenced of course by the availability of a reliable ground-truth that can assess the relation between FSC and the spectral behavior of the mixed pixel.

2.3 Challenges and gaps

The major challenge associated with mapping of snow cover in the Arctic is the lack of ground-validated datasets and an overall scarcity of dense, high quality image time series. Cloud cover and low sun elevation represent an important limitation to the availability of complete time-series concerning the snow cover. This gap can be filled by terrestrial photography that represents an important source of continuous and high-spatially resolved description of the FSC conditions. The integration of different snow products, obtained at different time and spatial resolutions is a major challenge at high latitudes.

3 Vegetation mapping

3.1 Background

The Arctic biome is broadly divided into sub, low and high Arctic dictated by the ecological effects of latitude and climate spanning from the tundra-taiga-ecotone in the south to the polar deserts in the north (Bliss and Matveyeva, 1992). Walker et al. (2005) improved this broad classification by further subdividing the Arctic biome into five bioclimatic zones with detailed vegetation descriptions, following a roughly latitudinal gradient from warmest and most vegetated in the south to coldest and least vegetated in the north. In general, Arctic vegetation cover and species biodiversity decreases with increasing latitude and though biodiversity is low at the biome scale, at the community scale it is comparable to temperate grasslands and coniferous biomes (Bliss et al., 1981).

Recent research highlights the heterogeneous and non-linear vegetation change occurring at multiple spatial scales in terrestrial Arctic ecosystems (Bhatt et al., 2010; Bjorkman et al., 2017, 2015; Elmendorf et al., 2012). Remote sensing offers a tool that can capture landscape and biome scale responses of Arctic vegetation to climate change though limitations exist due to the often challenging acquisition conditions that limit data frequency and quality. The majority of mapping efforts provide rasterized ecological classifications or estimations of vegetation properties from local to biome scales through inferred relationships with broadband vegetation indices (VIs). However, heterogeneous species composition, dynamic surface moisture conditions, and an abundance of non-photosynthetic plant material and non-vascular species can complicate broadband VI signals, especially in sparsely vegetated areas (Liu et al., 2017).

Advancements of optical sensors in recent years (e.g. Sentinel-2, PRISMA) have increased both the spatial and spectral resolution of optical remote sensing imagery facilitating the use of narrowband indices and the entire spectral feature space of the electromagnetic spectrum. These new advanced systems can provide additional information to better capture and characterize vegetation properties and the complex changes occurring in terrestrial Arctic ecosystems.

Vegetation mapping can be divided into the two categories of land cover classification and estimation of vegetation properties. The most commonly used land cover map in the Arctic is the 14-km resolution Circumpolar Arctic Vegetation Map (CAVM; CAVM Team, 2003), a hierarchical classification of physiognomic units with detailed vegetation description derived from a combination of AVHRR spectral information and manual delineation by local experts. Recently,

a 1-km raster CAVM was developed which greatly improves the spatial resolution and detail of this highly valuable classification (Raynolds et al., 2019).

The identification of Arctic tundra vegetation species, plant functional types and/or vegetation communities is challenging due to a lack of standard definitions, circumpolar nomenclature and the spatial scale and detail of available data. The majority of other vegetation mapping efforts in the Arctic have been performed at regional or local scales produced through automated or semi-automated classification of satellite data combined with ancillary data such as terrain attributes, percent vegetation cover, aboveground biomass and soil moisture (Atkinson and Treitz, 2012; Fraser et al., 2012; Johansen et al., 2012).

Mapping Arctic tundra vegetation properties is largely dependent on inferred relationships with broadband vegetation indices. A lot of uncertainty remains in estimating vegetation properties given the scarcity of high quality validation datasets. However at local and regional scales in multiple Arctic ecosystems, ground-validated satellite-derived vegetation indices have been used to successfully estimate and map aboveground biomass, leaf-area index (LAI), phenology, productivity and more recently solar-induced fluorescence (Raynolds et al., 2012; Williams et al., 2008; Shaver et al., 2013; Emmerton et al., 2016; Walther et al., 2018).

To date there are very few vegetation mapping efforts using Sentinel-2 in terrestrial Arctic ecosystems though it has been identified as an important sensor for a wide range of mapping applications (Bartsch et al., 2016). Riihimäki et al. (2019) demonstrated that both Sentinel-2 and Landsat 8 OLI are capable of estimating fractional vegetation cover in a sub Arctic tundra ecosystem with high accuracy. Mochalov et al. (2019) used Sentinel-2 in combination with field data and botanical information as an input in a machine-learning algorithm to accurately map vegetation communities in Siberian tundra. Langford et al. (2019) also demonstrated the potential of machine-learning to improve vegetation classification using convolutional neural networks with Landsat 8 OLI, hyperspectral and terrain datasets to accurately map vegetation at a 5 m scale in western Alaska. Many studies also incorporate Landsat 8 OLI into long-term Landsat time series for multiple applications of mapping Arctic vegetation (Frost et al., 2014; Macander et al., 2017; Edwards and Treitz, 2015).

3.2 Case Study

3.2.1 2.2.1 Lena Delta biomass and biodiversity

As part of the iCUPE project, the application of Sentinel-2 and Landsat-8 data to questions of Arctic vegetation change is expanded by relating spectral information of the sensors to destructively sampled biomass and biodiversity data in the central Lena Delta, Siberia (Figure 3-1). A dense time-series of Sentinel-2 and Landsat 8 was collected over the region in the growing season of 2018 and concurrent biomass and plant species data were collected. The influence of phenology, topography, and vegetation community type will be taken into account. The results will increase the availability of ground-validated biomass datasets for extrapolation and use in the multidisciplinary research of the iCUPE project.

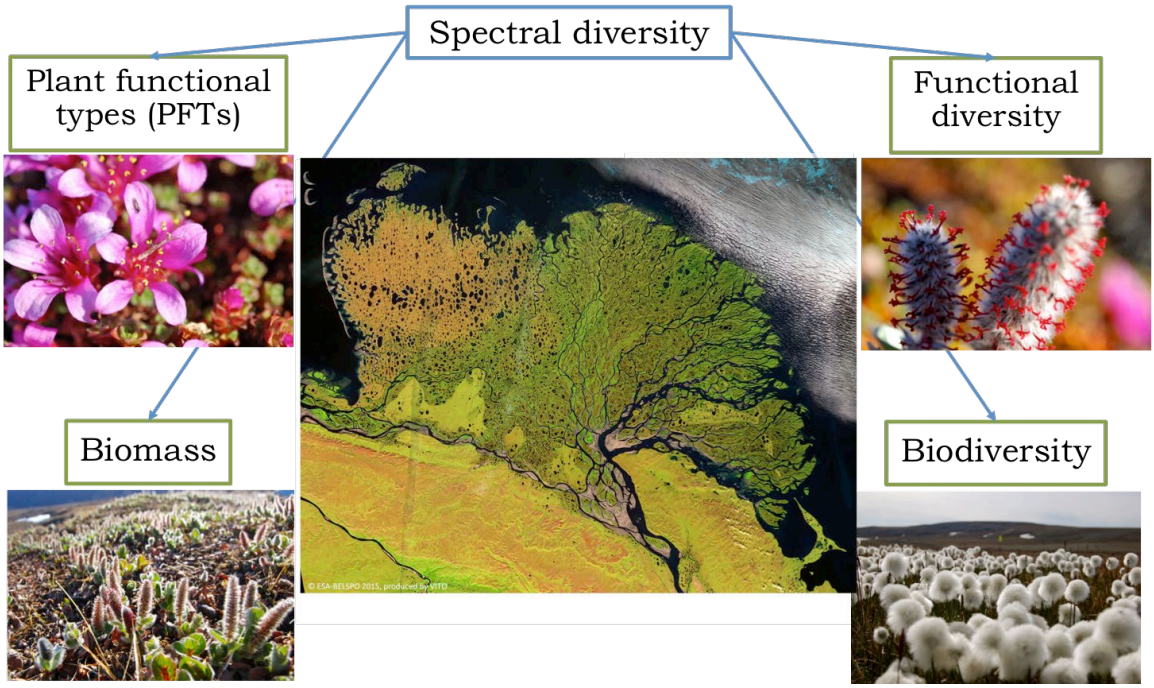

Figure 3-1 Sentinel-2 image of the central Lena Delta and the extractable vegetation variables using spectral diversity measures. © ESA-BELSPO 2015, produced by VITO

Most of the high spectral resolution studies of Arctic vegetation used ground-based hypersepctral spectral data (Beamish et al., 2017; Huemmrich et al 2013; Bratsch et al., 2016; Buchhorn et al., 2013; Liu et al., 2017). A small number of studies exist using Hyperion-EO but the data quality and latitudinal extent is limited (Langford et al., 2019). The quantity and quality of hyperspectral data is increasing, providing the opportunity to use these advanced missions to better characterize Arctic vegetation.

3.2.2 North Slope Alaska photosynthetic pigments and plant functional types

In preparation for hyperspectral satellite and aerial data acquisitions, a detailed ground-based spectral characterization of low Arctic tundra vegetation on the Alaskan North Slope was conducted (Beamish et al., 2017; Beamish et al., 2018). We collected canopy-based spectral reflectance in five dominant low Arctic vegetation communities at three major phenological phases of leaf-out, maximum canopy, and senescence (Figure 3-2). As a first step to improve the estimation and monitoring of Arctic tundra vegetation we examined within and between community variability to determine the most discriminative wavelengths and phenological phase. The results suggest that for imaging spectroscopy, the senescent phase data is superior to early and peak season for differentiating vegetation communities (Beamish et al., 2017).

In a second step, the spectral reflectance data were then compared to simple greenness ratios from digital cameras and photosynthetic pigments extracted from dominant plant species to understand how vegetation colour reflects vegetation change. Results indicate that shifts in vegetation colour are concurrent with shifts in photosynthetic pigment content and simple greenness ratios can be used to estimate pigment concentrations (Beamish et al., 2018).

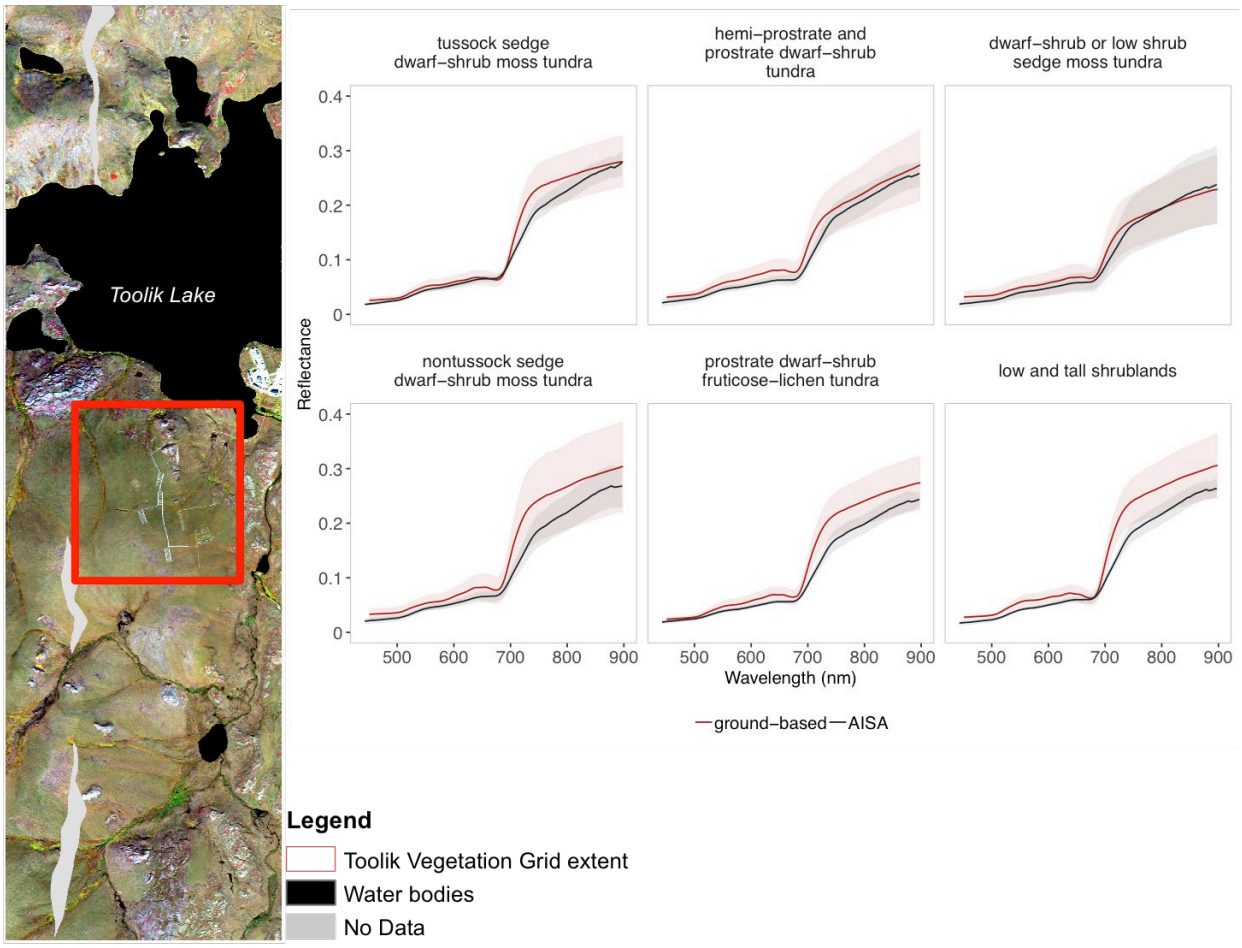

Figure 3-2 Airborne hyperspectral AISA orthomosaic of the Toolik Lake Natural Research Area. Spectral characterization at the ground and airborne scale of six dominant vegetation communities. Moisture, stature and fractional cover of plant functional types influenced spectral scaling.

In a final step, using detailed plant compositional data, we explored the sensitivity using simple linear regression of individual wavelength and two-band spectral indices to varying fractional vegetation cover (Figure 3-3). We found that wavelengths and spectral indices showed overlapping areas of sensitivity to vascular and non-vascular functional types which could confound the extraction of vegetation properties derived from vegetation indices.

These results overall suggest that using wavelengths and narrowband indices in the visible spectrum can provide sufficient information to monitor seasonal changes in vegetation activity and vitality. This reduces the dependency on the near infrared which has shown high sensitivity to surface moisture, a ubiquitous feature in Arctic tundra ecosystems. In addition, phenology clearly plays an important role in differentiating vegetation communities and deriving vegetaiton properties.

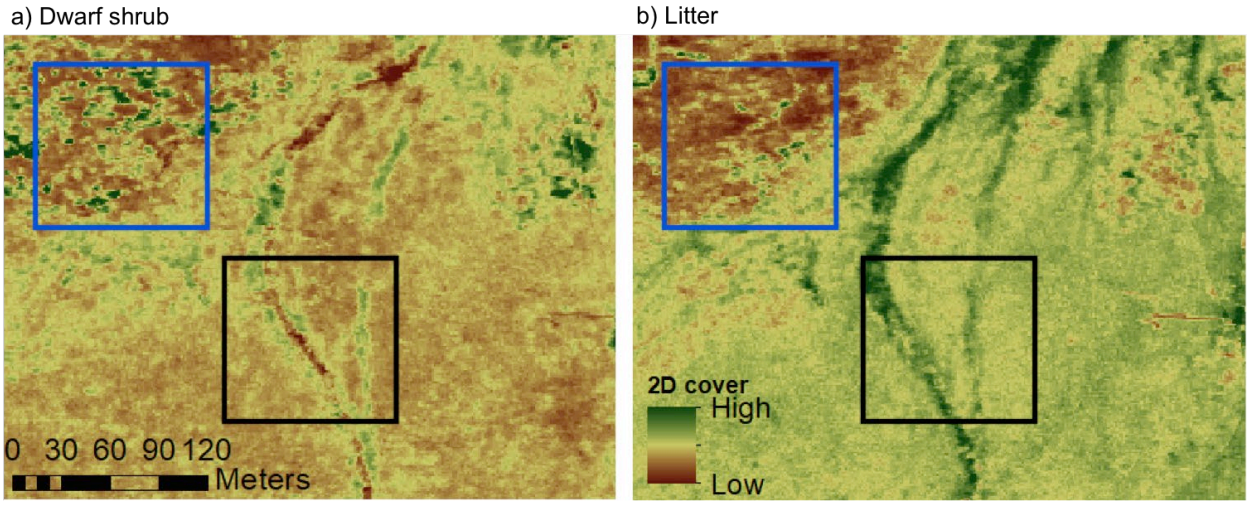

Figure 3-3 Mapping plant functional types at the airborne scale in two distinct geomorphic areas, dry upland heath and wet shrubby water tracks. At the airborne scale, extraction of dwarf shrub cover was poor in the water tracks but good in the upland heath.

3.3 Challenges and gaps

The major challenge associated with mapping of Arctic vegetation is the lack of ground-validated datasets and an overall scarcity of dense, high quality image time series. The increasing availability of hyperspectral data will face similar challenges and given the limited number of hyperspectral remote sensing studies in the Arctic, high quality, ground-validated data is required to accurately interpret these dense and complex datasets. The rise of more advanced classification methods such as machine-learning techniques are highly promising for Arctic vegetation mapping using advanced remote sensing platforms. An increased effort to develop Arctic-specific algorithms is needed.

4 Artificial light

4.1 Background

One of the defining features of Arctic regions is the unique light cycle. In contrast to temperate and tropical latitudes, Arctic regions are famous for experiencing long periods of “midnight sun” during the summer, and aurora during winter when the sun is set. Less well known, but likely of great importance for Arctic animals, are the periods in winter during which the full moon does not set for multiple days. For example, Last et al. (2016) demonstrated that vertical migration of zooplankton due to lunar cycles is ubiquitous across the Arctic Ocean. Artificial light at human habitations is far brighter than light from the aurora and the moon, and therefore has the potential to dramatically impact the behaviour and physiology of Arctic animals. Ludvigsen et al. (2018) hypothesize that the susceptibility of Arctic animals to light pollution is at its extreme in this region.

Artificial light could potentially affect Arctic animals in at least two ways. First, is the effect of artificial light on orientation, navigation, and hunting. Ludvigsen et al. (2018) demonstrated that the light polluted environment near research vessels in Arctic waters affects zooplankton communities to a degree where it is impossible to examine the abundance and natural rhythms within the upper 100 m of the water column. Second, Arctic animal and plant physiology is specially adapted for the region, and exposure to light during polar night could impact seasonal biology. Stokkan et al. (2013) showed that Arctic reindeer adjust their tapetum lucidum (reflector system regulating light sensitivity in the eyes) between winter and summer. In wild populations, it is golden in summer and deep blue in winter. However, reindeer kept at the University of Tromsø were observed to have green tapetum lucidum all winter, presumably due to their exposure to artificial light from distant urban light and its reflection from clouds.

The polar environment has important effects for both the propagation of light in the environment, and for observations of artificial light from space. As mentioned above, clouds typically brighten rather than darken the night sky near lit areas (Kyba et al., 2011), but this effect is especially pronounced in the arctic, due to the high albedo of snow cover (Jechow & Hölker, 2019). The seasonal cycle also means that in contrast to temperate areas, artificial light can only be observed from October-March, with observations at higher latitudes possible only from November-February, periods when snow cover is near certain. Furthermore, because polar orbiting satellites pass over polar regions more frequently, the number of possible observations per day is larger. For example, in December, the Visible Infrared Imaging Radiometer Suite

Day/Night Band (DNB) on the Suomi Net Primary Productivity (NPP) satellite images areas at the equator approximately once per night, compared to 60° and 70° with approximately 2.5 and 4 overpasses per night, respectively.

Artificial light emissions are strongly connected with human activity around the world, and the Arctic is no exception. Light sources in the Arctic include human habitations, resource extraction sites (e.g. from gas flaring), and air and sea ports. Many of these lights are continuously on and are therefore visible during the late-night overpasses of Suomi NPP. In this report, we present three case studies regarding artificial light emissions in the Arctic. The first is intended to demonstrate how a tool developed in the ERA-PLANET GEO-Essential project can be used to examine light changes in the Arctic. The second is an analysis of the types of artificial light sources on the Yamal Peninsula. The third is an analysis of how the artificial light environment is changing across the entire Arctic.

4.2 Case studies

4.2.1 Colville Delta

The “Radiance Light Trends” web application makes it possible to quickly analyze trends in night lights in a browser without needing to download the satellite dataset or run GIS software (Figure 4-1). The application is based on DNB data processed by the Earth Observation Group of the Colorado School of Mines (https://eogdata.mines.edu/download_dnb_composites.html). It can immediately be seen that the aurora produces significant light in Arctic regions, introducing a background that complicates the identification of areas with low levels of artificial light (e.g. small villages). Nevertheless, brighter and larger sources of artificial light are easily seen, for example in the case of resource extraction in the Colville River Delta, Alaska (Figure 4-2), where artificial light associated with oil and gas extraction is easily visible above the background.

In Figure 3.2, a region at the extreme West of the light producing region was selected. Figure 4-3 shows the lighting trend for the average value of DNB data from this region during 2012-2019. A clear transition in the light emissions of the site can be seen, with artificial light emissions beginning at the end of 2015. The figure also shows that the observed radiance is not identical from month to month. The causes of variations in monthly night emissions are discussed by Coesfeld et al. (2018). In the case of the Arctic, the freshness of snow cover plays an especially strong role.

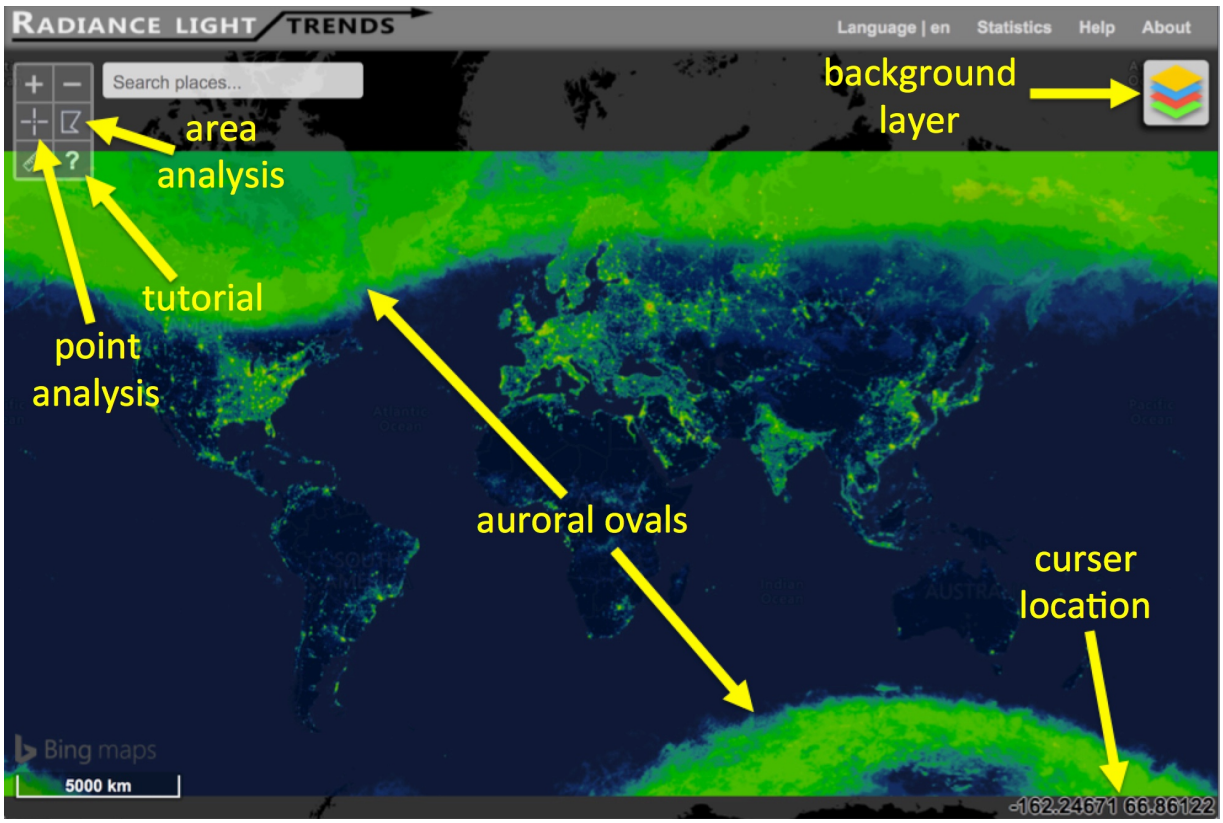

Figure 4-1 Main page of the Radiance Light Trends application, with annotations in yellow highlighting several features. The EOG annual composite DNB image for 2016 is shown.

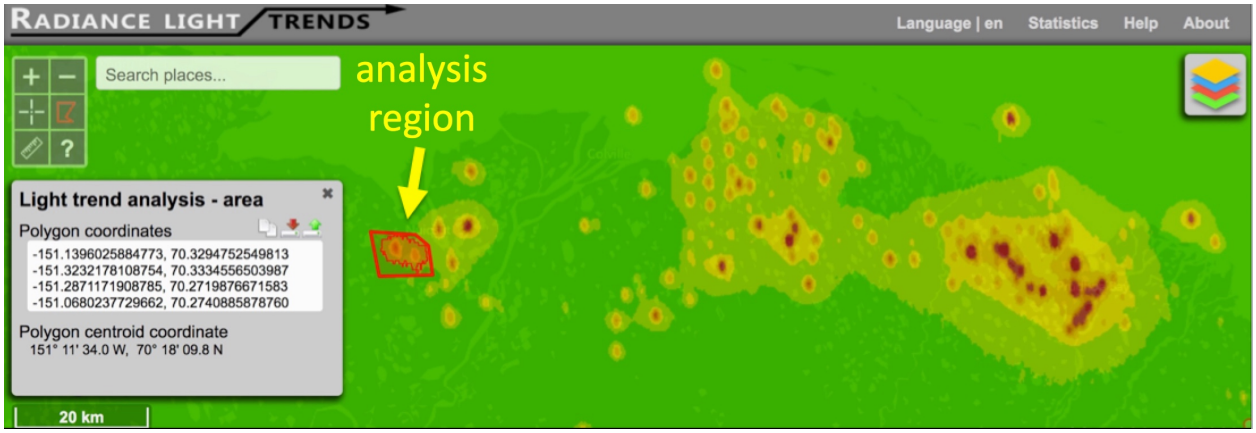

Figure 4-2 Zoom in of the Colville Delta region. The lights layer is the EOG annual composite for 2016. The yellow arrow shows the location of a region to be analyzed. The red outline inside the analysis region shows the area that EOG determined to have regular light emissions (i.e. not background light). The coordinates of polygons drawn by a user can be downloaded, and then uploaded later to repeat the analysis.

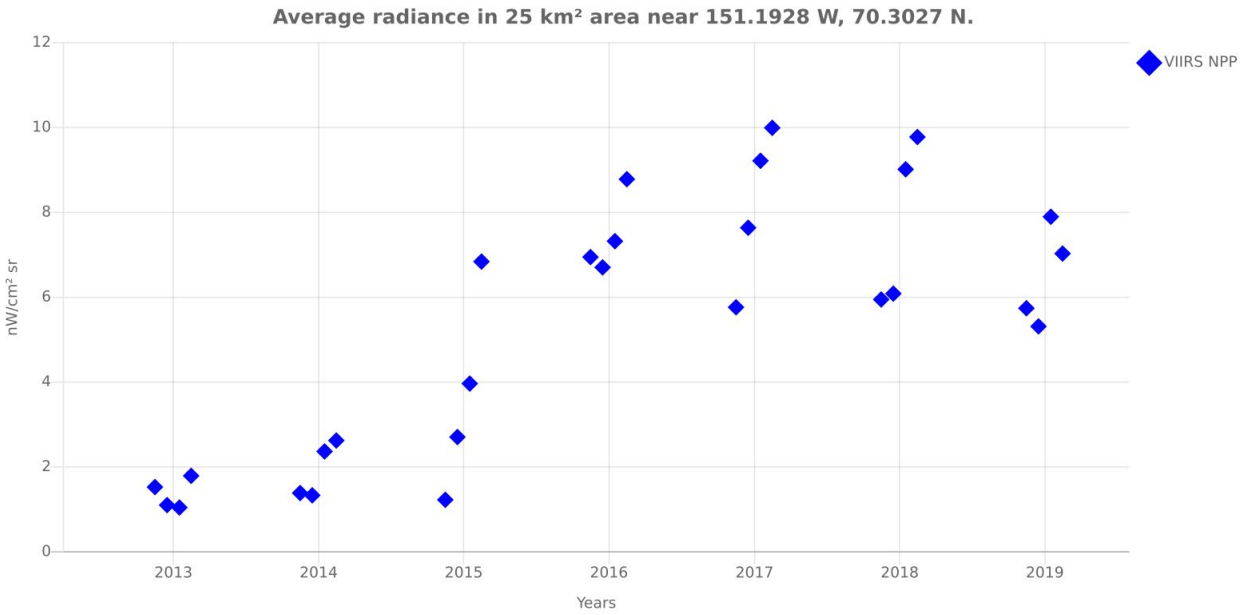

Figure 4-3 Change in average light observed in the selected region shown in Figure L1. Because of the high latitude, data were only available during November through February.

4.2.2 Yamal Peninsula

The Radiance Light Trends app was used to identify artificial light sources on the Yamal Peninsula in Russia, and then visible band daytime imagery from Google Maps and Bing Maps was used to identify what type of human activity was responsible for the light. The positions of the 78 lit areas and their light source classification are shown in Figure 4-4; a CSV file describing the sites is available in Coesfeld & Kyba (2019), as is a KMZ file for viewing the sites in Google Earth or another viewer. The most common type of land use associated with light emissions were areas related to oil and gas extraction and/or refining (classified as industry and industry/flare). There is a string of artificial lights with points separated at 30-40 km distance associated with a road, and seven communities. In ten cases, high resolution imagery was either not available or out of date, so the site was classified as unknown. Water indicates lights that are not on land, most likely indicating an offshore platform.

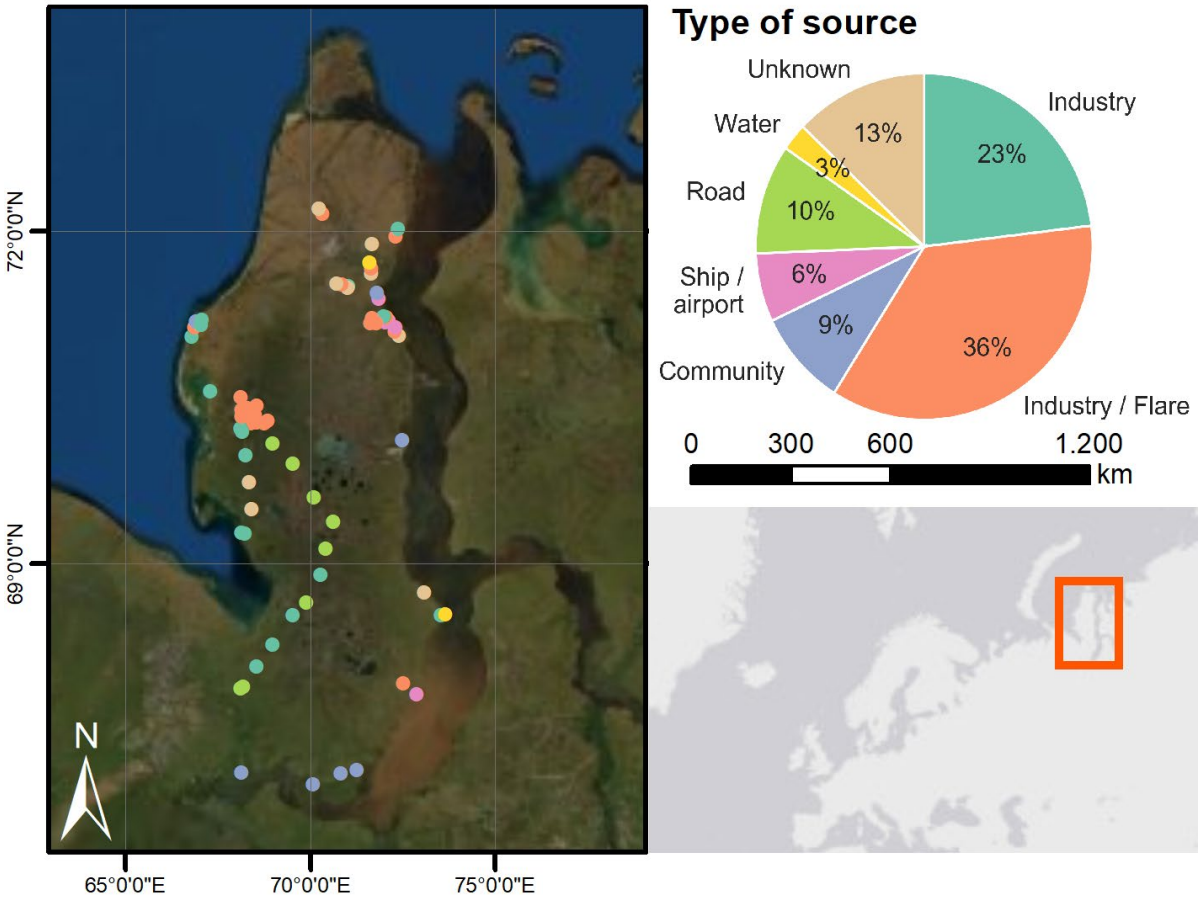

Figure 4-4 Locations and categorization of artificial light sources on the Yamal Peninsula. Background maps are Esri basemaps: World Imagery (left) and World Light Gray Canvas (right).

3.2.3 Changes in lit regions across the entire Arctic

As a final case study, we consider how the number of lit areas and their size are changed across the Arctic over a seven year period. We did not examine what sources were responsible for observed trends. In this case, Radiance Light Trends was not used. Rather, DNB data were manually downloaded and examined in Python (scripts available in Coesfeld, 2019). Lights sources across the Arctic are shown in Figure 4-5. For this purpose, the boundary of the Arctic was defined as 60ºN. Pixels were considered lit if they had a radiance above a specified value in nW/cm^2sr, and areas with adjacent lit pixels were agglomerated into individual “lit sites”.

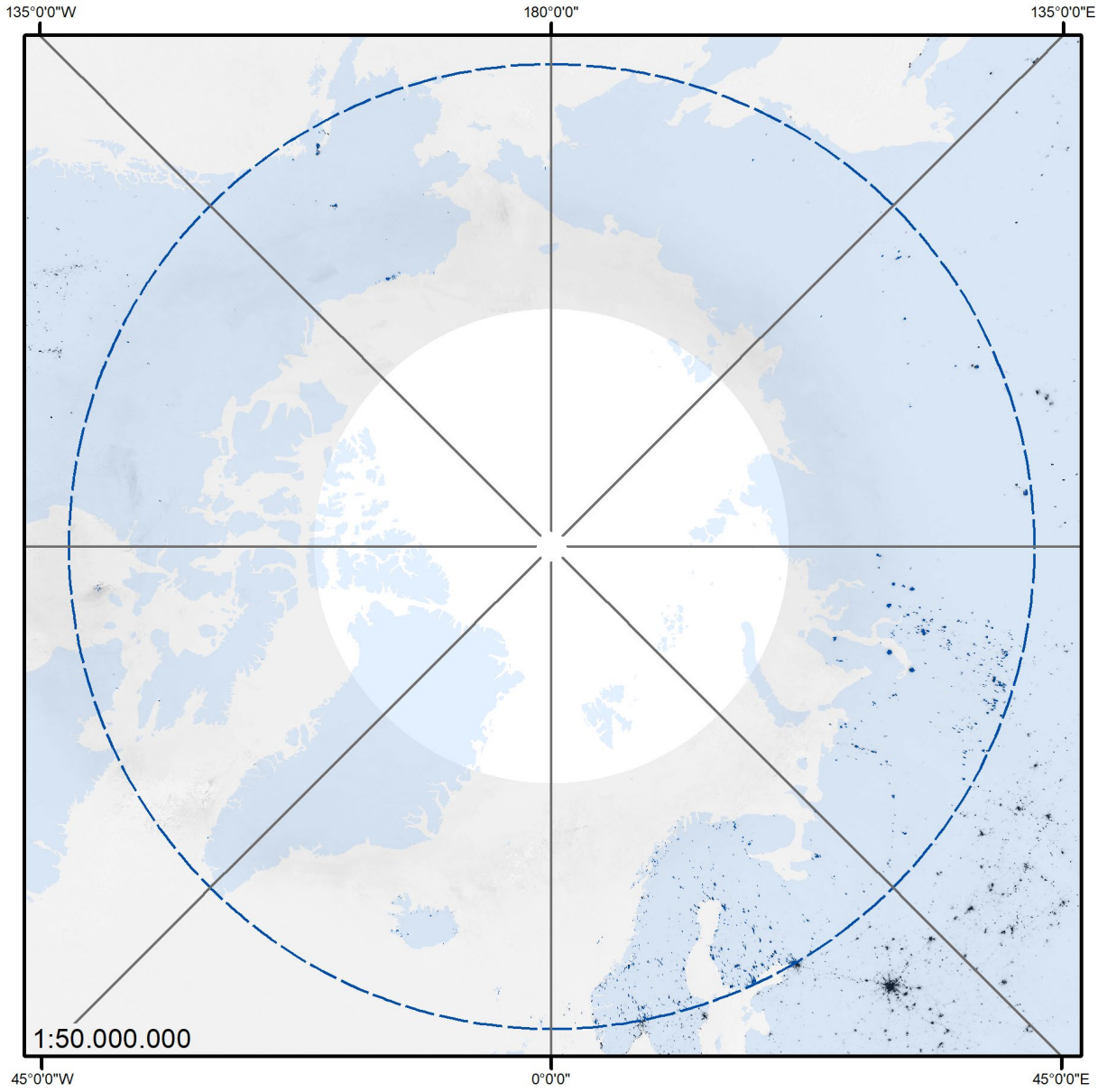

Figure 4-5 Artificial light sources in and near to the Arctic in December, 2018. The dashed blue line shows 60° North, light sources are shown in black. The land areas are shaded based on maps from Natural Earth's free vector and raster map data available at naturalearthdata.com. The EOG maps do not include latitudes above 75° North, so any lights that are located there are not shown (white area at center).

Each monthly dataset from the EOG was analyzed individually for the months of November to February during the period for which data is available in 2012-2019. The trends in total number of lit sites and total lit area are shown in Figure 4-6 and Figure 4-7, respectively. Three radiance cuts of 5, 10, and 20 nW/cm2sr were analyzed separately. For both lit area and total number of lit sites, the data is most consistent with a fairly rapid increase. However, the variability in the satellite dataset remains too large to rule out the null hypothesis that lights are not increasing.

There is a very clear seasonal effect: The number of detected sites and their area are typically smallest in November, and larger with each subsequent month. This is not surprising, as snow cover increases during this period.

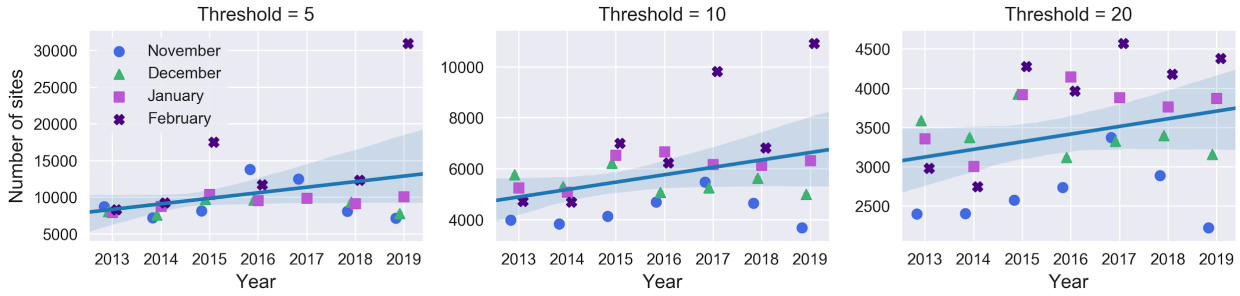

Figure 4-6 Total number of illuminated sites above 60°N in each of the DNB datasets for three different radiance thresholds (in nW/cm^{2}sr). Data from February, 2017 is not shown for the threshold of 5 nW/cm^{2}sr, due to a large upward fluctuation.

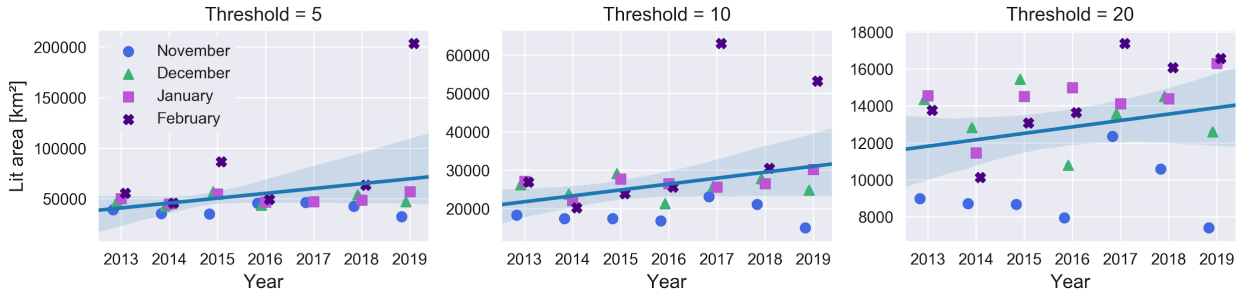

Figure 4-7 Total area of illuminated pixels above 60°N in each of the DNB datasets for three different radiance thresholds (in nW/cm^{2}sr). Data from February, 2017 is not shown for the threshold of 5 nW/cm^{2}sr, due to a large upward fluctuation.

4.3 Challenges and gaps

A key challenge for observing artificial light in the Arctic from space, particularly for smaller light installations, is the dramatic variability in atmospheric aurora and surface albedo (due to snow cover). This can be seen in the dramatic upward fluctuations in areas lit above 5 nW/cm^{2}sr observed in February of 2017 and 2019 (Figure 4-6 & Figure 4-7), and the pattern that more bright areas are typically detected in February than in November. Another difficulty is that night lights data are not acquired throughout the entire night, but rather early in the morning (local time). If electric lights are on only during the “day” and early evening hours, they may not be detected by DNB at all. While future night light detectors on geostationary satellites could observe the evolution of lights over the course of the night (Levin et al., 2019), such observations would be more challenging or impossible for polar regions because of the very low

elevation angle of the satellites relative to the horizon. Similarly, transient light sources (such as from moving ships) may impact arctic marine life, and may be difficult to distinguish from spikes in aurora. Finally, additional ground-based observations of light such as those undertaken by Jechow et al. (2019) would be valuable both for understanding the natural light environment of the polar night, and also the degree to which humans are changing it.

In closing, individuals and industry could minimize the environmental impact of artificial light emissions, while also reducing fuel use for producing electricity for the lights through changing practices. For example, Wren et al. (2015) documented how reducing light use on oil rigs through more careful direction of the lights can actually increase visibility for workers. This work led to a set of recommendations for lighting oil and gas infrastructure[1], which has been endorsed by key industry players, including the American Petroleum Institute and the Texas Oil & Gas Association. Other practices, such as minimizing flaring, turning off lights when not in use, and using only as much light as is needed, could similarly reduce the environmental impact of anthropogenic light on the polar night.

5 Conclusion

The case studies presented in this report demonstrate what a powerful tool optical remote sensing is for monitoring and characterizing diverse changes in terrestrial Arctic ecosystems. Both vegetation and night light mapping require in-situ validation to better understand regional and biome scale trends. Providing detailed ground-validated datasets from advanced multi and hyperspectral platforms will improve our understanding of the current state of snow, aboveground biomass, photosynthetic activity, and biodiversity. Such information is crucial for accurately monitoring and relating changes to other iCUPE work packages studying atmospheric chemistry, snow depth and snow melt dynamics, and urban and industrial development. Night light mapping is a highly valuable tool to monitor urban and industrial development and provide important information to monitor the ecological impact of anthropogenic activity to Arctic flora and fauna.

[1] available at: https://texanbynature.org/wp-content/uploads/2018/06/RecommendedLightingPracticesFINAL.pdf

6 References

AMAP, 2017. AMAP Assessment 2016: Chemicals of Emerging Arctic Concern. Arctic Monitoring and Assessment Programme (AMAP), Oslo, Norway. pp. xvi+353

Atkinson, D.M., Treitz, P., 2012. Arctic ecological classifications derived from vegetation community and satellite spectral data. Remote Sens. 4, 3948–3971. https://doi.org/10.3390/rs4123948

Barsi, J.A., Lee, K., Kvaran, G., Markham, B.L., Pedelty, J.A., 2014. The Spectral Response of the Landsat-8 Operational Land Imager. Remote Sens. 6, 10232–10251. https://doi.org/10.3390/rs61010232

Bartsch, A., Hofler, A., Kroisleitner, C., Trofaier, A.M., 2016. Land cover mapping in northern high latitude permafrost regions with satellite data: Achievements and remaining challenges. Remote Sens. 8. https://doi.org/10.3390/rs8120979

Beamish, A., Coops, N. C., Chabrillat, S., Heim, B. 2017. A phenological approach to spectral differentiation of low-arctic tundra vegetation communities, North Slope, Alaska. Remote Sens. 9 (11). https://doi.org/10.3390/rs9111200

Beamish, A., Coops, N. C., Hermosilla, T., Chabrillat, S., Heim, B. 2018. Monitoring pigment-driven vegetation changes in a low-Arctic tundra ecosystem using digital cameras. Ecosphere. 9 (2). https://doi.org/10.1002/ecs2.2123

Beniston, M., Farinotti, D., Stoffel, M., Andreassen, L.M., Coppola, E., Eckert, N., Fantini, A., Giacona, F., Hauck, C., Huss, M., 2018. The European mountain cryosphere: A review of its current state, trends, and future challenges. Cryosphere 12, 759–794. https://doi.org/10.5194/tc-12-759-2018

Bhatt, U.S., Walker, D., Raynolds, M.K., Comiso, J., Epstein, H., Jia, G.J., Gens, R., Pinzon, J., Tucker, C., Tweedie, C., Webber, P., 2010. Circumpolar Arctic tundra vegetation change is linked to sea ice decline. Earth Interact. 14, 1–20. https://doi.org/10.1175/2010EI315.1

Bjorkman, A.D., Elmendorf, S.C., Beamish, A.L., Vellend, M., Henry, G.H.R., 2015. Contrasting effects of warming and increased snowfall on Arctic tundra plant phenology over the past two decades. Glob. Chang. Biol. 21. https://doi.org/10.1111/gcb.13051

Bjorkman, A.D., Vellend, M., Frei, E.R., Henry, G.H.R., 2017. Climate adaptation is not enough: warming does not facilitate success of southern tundra plant populations in the high Arctic. Glob Chang. Biol 23, 1540–1551. https://doi.org/10.1111/gcb.13417

Bliss, L.C., Matveyeva, N. V, 1992. Circumpolar arctic vegetation. *Arctic ecosystems in a changing climate: an ecophysiological perspective.* Reynolds, J.F., and Svoboda, J., Chu, E.W. (Eds.). Academia Press, Inc., pp. 59–89.

Bratsch, S.N., Epstein, H., Buchhorn, M., Walker, D., Landes, H., 2017. Relationships between hyperspectral data and components of vegetation biomass in Low Arctic tundra communities at Ivotuk, Alaska. Environ. Res. Lett. 12. https://doi.org/10.1088/1748-9326/aa572e

Buchhorn, M., Walker, D., Heim, B., Raynolds, M.K., Epstein, H.E., Schwieder, M., 2013. Ground-based hyperspectral characterization of Alaska tundra vegetation along environmental gradients. Remote Sens. 5, 3971–4005. https://doi.org/10.3390/rs5083971

CAVM team, 2003. Circumpolar Arctic Vegetation Map. Scale 1: 7,500,000. Conservation of Arctic Flora and Fauna (CAFF) Map No. 1. US Fish and Wildlife Service.(Anchorage, AK). Available at http://www.geobotany.uaf.edu/cavm/.

Chapin, Sturm, Serreze, McFadden, Key, Lloyd, McGuire, Rupp, Lynch, Schimel, Ber- inger, Chapman, Epstein, Euskirchen, Hinzman, Jia, Ping, C.-L., Tape, Thompson, Walker, Welker, 2005. Role of Land-Surface Changes in Arctic Summer Warming. Science. 310, 657–660.

Coesfeld, J., Anderson, S., Baugh, K., Elvidge, C., Schernthanner, H., & Kyba, C. (2018). Variation of individual location radiance in VIIRS DNB monthly composite images. Remote Sens. 10(12), 1964. https://doi.org/10.3390/rs10121964

Coesfeld, J. (2019) Python scripts for identifying and clustering bright light sources in the Arctic (2019), Software publication by GFZ Data Services.

Coesfeld, J., Kyba, C.C.M. (2019) Classification of artificial light sources in the Yamal Peninsula, Data publication by GFZ Data Services, DOI: http://doi.org/10.5880/GFZ.1.4.2019.007

Dietz, A.J., Kuenzer, C., Gessner, U., Dech, S., 2011. Remote sensing of snow–A review of available methods. Int. J. Remote Sens. 33, 4094–4134. https://doi.org/10.1080/01431161.2011.640964

Dozier, J., Green, R.O., Nolin, A.W., Painter, T.H., 2009. Interpretation of snow properties from imaging spectrometry. Remote Sens. Environ. 113, 525–537. https://doi.org/10.1016/j.rse.2007.07.029

Edwards, R., Treitz, P., 2017. Vegetation Greening Trends at Two Sites in the Canadian Arctic: 1984–2015. Arctic, Antarct. Alp. Res. 49, 601–619. https://doi.org/10.1657/aaar0016-075

Elmendorf, S.C., Henry, G.H.R., Hollister, R.D., Björk, R.G., Bjorkman, A.D., Callaghan, T. V, Collier, L., Cooper, E.J., Cornelissen, J.H.C., Day, T.A., Fosaa, A., Gould, W.A., Grétarsdóttir, J., Harte, J., Hermanutz, L., Hik, D.S., Hofgaard, A., Jarrad, F., Jónsdóttir, I., Keuper, F., Klanderud, K., Klein, J.A., Koh, S., Kudo, G., Lang, S.I., Loewen, V., May, J.L., Mercado, J., Michelsen, A., Molau, U., H, M.I., Oberbauer, S.F., Pieper, S., Post, E., Rixen, C., Robinson, C.H., Schmidt, N., Shaver, G.R., Stenström, A., Tolvanen, A., Totland, Ø., Troxler, T., Wahren, C., Webber, P.J., Welker, J.M., Wookey, P.A., 2012. Global assessment of experimental climate warming on tundra vegetation: heterogeneity over space and time. Ecol Lett. 15, 164–175. https://doi.org/10.1111/j.1461-0248.2011.01716.x

Emmerton, C.A., St. Louis, V.L., Humphreys, E.R., Gamon, J.A., Barker, J.D., Pastorello, G.Z., 2016. Net ecosystem exchange of CO2 with rapidly changing high Arctic landscapes. Glob. Chang. Biol. 22, 1185–1200. https://doi.org/10.1111/gcb.13064

ESA, 2018. Sen2Cor configuration and user manual., HTTP://STEP.ESA.INT/THIRDPARTIES/SEN2COR/2.5.5/DOCS/S2-PDGS-MPC-L2A-SUM-V2.5.5_V2.PDF

Fraser, R., McLennan, D., Ponomarenko, S., Olthof, I., 2012. Image-based predictive ecosystem mapping in Canadian arctic parks. Int. J. Appl. Earth Obs. Geoinf. 14, 129–138. https://doi.org/10.1016/j.jag.2011.08.013

Frost, G. V., Epstein, H.E., 2014. Tall shrub and tree expansion in Siberian tundra ecotones since the 1960s. Glob. Chang. Biol. 20, 1264–1277. https://doi.org/10.1111/gcb.12406

Hall, D.K., Riggs, G.A., 2016. MODIS/[Terra/Aqua] Snow Cover Daily L3 Global 500m Grid, Version 6. NASA National Snow and Ice Data Center Distributed Active Archive Center. Available online: https://nsidc.org/data/modis/data_summaries (accessed on 1 October 2019).

Huemmrich, K.F., Gamon, J.A., Tweedie, C.E., Campbell, P.K.E., Landis, D.R., Middleton, 2013. Arctic Tundra Vegetation Functional Types Based on Photosynthetic Physiology and Optical Properties. IEEE J. Sel. Top. Appl. Earth Obs. Remote Sens. 6, 265–275. https://doi.org/10.1109/JSTARS.2013.2253446

IPCC, 2014: Climate Change 2014: Synthesis Report. Contribution of Working Groups I, II and III to the Fifth Assessment Report of the Intergovernmental Panel on Climate Change [Core Writing Team, R.K. Pachauri and L.A. Meyer (eds.)]. IPCC, Geneva, Switzerland, 151 pp.

Jechow, A., & Hölker, F. (2019). Snowglow—The Amplification of Skyglow by Snow and Clouds Can Exceed Full Moon Illuminance in Suburban Areas. J. Imaging, 5(8), 69. https://doi.org/10.3390/jimaging5080069

Johansen, B.E., Karlsen, S.R., Tømmervik, H., 2012. Vegetation mapping of Svalbard utilising Landsat TM/ETM+ data, in: Polar Rec. pp. 47–63. https://doi.org/10.1017/S0032247411000647

Kyba, C. C., Ruhtz, T., Fischer, J., & Hölker, F. (2011). Cloud coverage acts as an amplifier for ecological light pollution in urban ecosystems. PloS One, 6(3), e17307. https://doi.org/10.1371/journal.pone.0017307

Langford, Z., Kumar, J., Hoffman, F.M., Norby, R.J., Wullschleger, S.D., Sloan, V.L., Iversen, C.M., 2016. Mapping Arctic plant functional type distributions in the Barrow environmental observatory using World View-2 and LiDAR datasets. Remote Sens. 8, 733. https://doi.org/10.3390/rs8090733

Last, K. S., Hobbs, L., Berge, J., Brierley, A. S., & Cottier, F. (2016). Moonlight drives ocean-scale mass vertical migration of zooplankton during the Arctic winter. Curr. Biol. 26(2), 244-251. https://doi.org/10.1016/j.cub.2015.11.038

Levin, N., Kyba, C. C., Zhang, Q., Sánchez de Miguel, A., Román, M. O., et al., (2019). Remote sensing of night lights: a review and an outlook for the future. Remote Sens. Environ. in press.

Liu, N., Budkewitsch, P., Treitz, P., 2017. Examining spectral reflectance features related to Arctic percent vegetation cover: Implications for hyperspectral remote sensing of Arctic tundra. Remote Sens. Environ. 192, 58–72. https://doi.org/10.1016/j.rse.2017.02.002

Ludvigsen, M., Berge, J., Geoffroy, M., Cohen, J. H., Pedro, R., Nornes, S. M., & Johnsen, G. (2018). Use of an Autonomous Surface Vehicle reveals small-scale diel vertical migrations of zooplankton and susceptibility to light pollution under low solar irradiance. Sci. Adv. 4(1), eaap9887. https://doi.org/10.1126/sciadv.aap9887

Macander, M.J., Frost, G. V., Nelson, P.R., Swingley, C.S., 2017. Regional quantitative cover mapping of tundra plant functional types in Arctic Alaska. Remote Sens. 9, 1024. https://doi.org/10.3390/rs9101024

Main-Knorn, M., Pflug, B., Louis, J., Debaecker, V., Gascon, F., Muller-Wilms, U., 2017. Sen2Cor for Sentinel-2. In: Proceedings of SPIE, 10427, 1-13. SPIE. Remote Sens. 11-14. https://doi.org/10.1:117/12.227821

Metsämäki, S.; Mattila, O.P.; Pulliainen, J.; Niemi, K.; Luojus, K.; Böttcher, K., 2012. An optical reflectance model-based method for fractional snow cover mapping applicable to continental scale. Remote Sens. Environ. 123, 508–521. https://doi.org/10.1016/j.rse.2012.04.010

Metsämäki, S.; Pulliainen, J.; Salminen, M.; Luojus, K.; Wiesmann, A.; Solberg, R.; Böttcher, K.; Hiltunen, M.; Ripper, E., 2015. Introduction to GlobSnow Snow Extent products with considerations for accuracy assessment. Remote Sens. Environ. 156, 96–108. https://doi.org/10.1016/j.rse.2014.09.018

Mochalov, V.F., Grigorieva, O. V., Zelentsov, V.A., Markov, A. V., Ivanets, M.O., 2019. Intelligent Technologies and Methods of Tundra Vegetation Properties Detection Using Satellite Multispectral Imagery. Springer, Cham, pp. 234–243. https://doi.org/10.1007/978-3-030-19813-8_24

Painter, T.H., Dozier, J., Roberts, D.A., Davis, R.E., Green, R.O., 2003. Retrieval of subpixel snow-covered area and grain size from imaging spectrometer data. Remote Sens. Environ. 85, 64–77. https://doi.org/10.1016/S0034-4257(02)00187-6

Painter, T.H., Rittger, K., McKenzie, C., Slaughter, P., Davis, R.E., Dozier, J., 2009. Retrieval of subpixel snow-covered area and grain size from imaging spectrometer data. Remote Sens. Environ. 113, 868–879. https://doi.org/10.1016/S0034-4257(02)00187-6

Raynolds, M.K., Walker, D.A., Balser, A., Bay, C., Campbell, M., Cherosov, M.M., Daniëls, F.J.A., Eidesen, P.B., Ermokhina, K.A., Frost, G. V., Jedrzejek, B., Jorgenson, M.T., Kennedy, B.E., Kholod, S.S., Lavrinenko, I.A., Lavrinenko, O. V., Magnússon, B., Matveyeva, N. V., Metúsalemsson, S., Nilsen, L., Olthof, I., Pospelov, I.N., Pospelova, E.B., Pouliot, D., Razzhivin, V., Schaepman-Strub, G., Šibík, J., Telyatnikov, M.Y., Troeva, E., 2019. A raster version of the Circumpolar Arctic Vegetation Map (CAVM). Remote Sens. Environ. https://doi.org/10.1016/j.rse.2019.111297

Raynolds, M.K., Walker, D., Epstein, H.E., Pinzon, J.E., Tucker, C.J., 2012. A new estimate of tundra-biome phytomass from trans-Arctic field data and AVHRR NDVI. Remote Sens. Lett. 3, 403–411. https://doi.org/10.1080/01431161.2011.609188

Riggs, G., Hall, D., Román, M.O., 2015. VIIRS Snow Cover Algorithm Theoretical Basis Document (ATBD), ver 1.0 https://viirsland.gsfc.nasa.gov/PDF/VIIRS_snow_cover_ATBD_2015.pdf

Riihimäki, H., Heiskanen, J., Luoto, M., 2017. The effect of topography on arctic-alpine aboveground biomass and NDVI patterns. Int. J. Appl. Earth Obs. Geoinf. 56, 44–53. https://doi.org/10.1016/j.jag.2016.11.005

Rodell, M., Houser, P.R, 2004. Updating a land surface model with MODIS-derived snow cover. J. Hydrometeorol., 5, 1064–1075. https://doi.org/10.1175/JHM-395.1

Salomonson, V.V., Appel, I, 2006. Development of the Aqua MODIS NDSI fractional snow cover algorithm and validation results. IEEE Trans. Geosci. Remote. 44, 1747–1756. https://doi.org/10.1109/TGRS.2006.876029

Salzano, R., Lanconelli, C., Salvatori, R. et al., Rend. Fis. Acc. Lincei (2016) 27(Suppl 1): 137. https://doi.org/10.1007/s12210-016-0513-y

Salzano R., Salvatori R, Valt M, Giuliani G, Chatenoux B and Ioppi L, (2019). Automated Classification of Terrestrial Images: The Contribution to the Remote Sensing of Snow Cover. Geosciences 2019, 9, 97; https://doi.org/10.3390/geosciences9020097

Shaver, G.R., Rastetter, E.B., Salmon, V., Street, L.E., van de Weg, M.J., Rocha, A., van Wijk, M.T., Williams, M., 2013. Pan-Arctic modelling of net ecosystem exchange of CO2. Philos. Trans. R. Soc. B Biol. Sci. 368, 20120485. https://doi.org/10.1098/rstb.2012.0485

Serreze, M., Walsh, J., III, C.F., Osterkamp, T., Dyurgerov, M., Romanovsky, V., Oechel, W., Morison, J., Zhang, T., Barry, R., 2000. Observational evidence of recent change in the northern high-latitude environment. Climatic Change 46, 159–207. https://doi.org/ 10.1023/a:1005504031923

Solberg, R., Amlien, J., Koren, H., 2006. A Review of Optical Snow Cover Algorithms. Norwegian Computing Center Note, SAMBA/40/06. 2006. Available online: https://www.nr.no/directdownload/4400/Solberg_-_A_review_of_optical_snow_algorithms.pdf.

Stokkan, K.A., Folkow, L., Dukes, J., Neveu, M., Hogg, C., Siefken, S., Dakin, S.C. and Jeffery, G., 2013. Shifting mirrors: adaptive changes in retinal reflections to winter darkness in Arctic reindeer. Proceedings of the Royal Society B: Biological Sciences, 280(1773), p.20132451. Stokkan, K.A., Folkow, L., Dukes, J., Neveu, M., Hogg, C., Siefken, S., Dakin, S.C. and Jeffery, G., 2013. Shifting mirrors: adaptive changes in retinal reflections to winter darkness in Arctic reindeer. P. Roy. Soc. B-Biol. Sci. 280(1773), p.20132451. https://doi.org/10.1098/rspb.2013.2451

Tedesco, M., Kokhanovsky, A.A., 2007. The semi-analytical snow retrieval algorithm and its application to MODIS data. Remote Sens. Environ. 111: 228–241. https://doi.org/10.1016/j.rse.2007.02.036

Vermote, E.F., Tanre, D., Deuze, J.L., Herman, M., Morcette, J.J., 1997. Second simulation of the satellite signal in the solar spectrum, 6S: An overview. IEEE Trans. Geosci. Remote, 35, 675–686. https://doi.org/10.1109/36.581987

Vermote, E., Justice, C., Claverie, M., Franch, B., 2016. Preliminary analysis of the performance of the Landsat 8/OLI land surface reflectance product. Remote Sens. Environ. 185. 46-56. https://doi.org/10.1016/j.rse.2016.04.008

Walker, D., Raynolds, M.K., Daniëls, F., Einarsson, E., Elvebakk, A., Gould, W.A., Katenin, A.E., Kholod, S.S., Markon, C.J., Melnikov, E.S., Moskalenko, N.G., Talbot, S.S., Yurtsev, B., 2005. The Circumpolar Arctic vegetation map. J. Veg. Sci. 16, 267–282. https://doi.org/10.1111/j.1654-1103.2005.tb02365.x

Walther, S., Guanter, L., Heim, B., Jung, M., Duveiller, G., Wolanin, A., Sachs, T., 2018. Assessing the dynamics of vegetation productivity in circumpolar regions with different satellite indicators of greenness and photosynthesis. Biogeosciences 15, 6221–6256. https://doi.org/10.5194/bg-15-6221-2018

Warren, S.G., Wiscombe, W.J., 1980. A model for the spectral albedo of snow, II, Snow containing atmospheric aerosols. J Atmos Sci 37(12):2734–2745. https://doi.org/10.1175/1520-0469(1980)037<2734:AMFTSA>2.0.CO;2

Warren, S.G., 1982. Optical properties of Snow. Rev. Geophys. 20(1): 67–89. https://doi.org/10.1029/RG020i001p00067

Williams, M., Bell, R., Spadavecchia, L., Street, L.E., Van Wijk, M.T., 2008. Upscaling leaf area index in an Arctic landscape through multiscale observations. Glob. Chang. Biol. 14, 1517–1530. https://doi.org/10.1111/j.1365-2486.2008.01590.x

Wiscombe, W.J., Warren, S.G. (1980). A model for the spectral albedo of snow. I: Pure snow. J. Atmo. Sci. 37(12): 2712–2733. https://doi.org/10.1175/1520-0469(1980)037%3C2712:AMFTSA%3E2.0.CO;2

WMO, 2010. World Meteorological Organization report, No. 1074

WMO, 2011. World Meteorological Organization report, No. 1085

Wren, B., & Locke, S. (2015). Upgraded Rig Lighting Improves Night Time Visibility While Reducing Stray Light and the Threat to Dark Skies in West Texas. In *SPE E&P Health, Safety, Security and Environmental Conference-Americas*. Society of Petroleum Engineers.

Yin, D., Cao, X., Chen, X., Shao, Y., Chen, J., 2013. Comparison of automatic thresholding methods for snow-cover mapping using Landsat TM imagery. Int. J. Remote Sens. 34, 6529–6538. https://doi.org/10.1080/01431161.2013.803631